Longitudinal map of transcriptome changes in the Lyme pathogen *Borrelia burgdorferi* during tick-borne transmission

Anne L. Sapiro[1*], Beth M. Hayes[1], Regan F. Volk[2], Jenny Y. Zhang[1], Diane M. Brooks[3], Calla Martyn[1], Atanas Radkov[1], Ziyi Zhao[1], Margie Kinnersley[3], Patrick R. Secor[3], Balyn W. Zaro[2], Seemay Chou[1*]

1 Department of Biochemistry & Biophysics, University of California, San Francisco, California, USA
2 Department of Pharmaceutical Chemistry and Cardiovascular Research Institute, University of California, San Francisco, California, USA
3 Division of Biological Sciences, University of Montana, Missoula, Montana, USA

*Corresponding authors:
Anne L. Sapiro: annesapiro@gmail.com & Seemay Chou: seemaychou@gmail.com

ABSTRACT

Borrelia burgdorferi (*Bb*), the causative agent of Lyme disease, must adapt to vastly different environments as the bacterium cycles between the tick vector and a vertebrate host. During a bloodmeal, *Bb* migrates from the tick midgut to the salivary glands and changes its gene expression, priming *Bb* for vertebrate infection. These tick-specific transmission events are dependent on key transcriptional regulators; however, the full range of transcriptional changes that occur over several days inside of the tick are technically challenging to capture. We developed an experimental approach to enrich *Bb* cells from *Ixodes* ticks during a transmitting bloodmeal to longitudinally define their global transcriptomic landscape. We identified 192 genes that substantially change expression over the course of the tick bloodmeal, most of which were located on plasmids of the *Bb* genome. The majority of upregulated genes encode proteins found at the cell envelope or proteins of unknown function, including 45 outer surface lipoproteins embedded in the unusual protein-rich coat of *Bb*. As these proteins may facilitate *Bb* interactions with host tissues or immune systems, we also utilized mass spectrometry to identify candidate tick proteins that physically associate with *Bb*. The *ex vivo Bb* transcriptomes and candidate tick interacting proteins presented here provide an important roadmap for investigating key determinants of *Bb* priming and transmission during the tick stage of its unique transmission cycle.

INTRODUCTION

Vector-borne microbial pathogens are transmitted by the bite of arthropods and have evolved sophisticated ways to adapt to vastly different environments as they move between vector and host. Uncovering their adaptive mechanisms can not only open avenues for disrupting pathogen transmission but also provide fundamental insights into vector physiology and microbial symbioses (Shaw and Catteruccia, 2018). Lyme disease, the most reported vector-borne disease in North America, is caused by the bacterial pathogen *Borrelia burgdorferi* (*Bb*) (Rosenberg et al., 2018; Steere et al., 2016). Its primary vector, the blacklegged tick *Ixodes scapularis,* acquires and transmits *Bb* through two separate multi-day bloodmeals, one in which *Bb* is acquired from an infected vertebrate host and a second, during the subsequent life stage, in which *Bb* is transmitted to a new host (Tilly et al., 2008). During the transmission bloodmeal, *Bb* proliferate in the tick midgut before a subset of these cells disseminate to the salivary glands (Dunham-Ems et al., 2009). *Bb* is deposited into the new host via the tick saliva extruded into the bite site (Spielman et al., 1987). Given the prolonged nature of *I. scapularis* feeding, the high specificity of vector-pathogen relationships, and the complicated array of events needed for successful *Bb* transmission, the tick bloodmeal provides an opportune intervention point for preventing pathogen spread. However, we do not currently have a clear understanding of the molecular mechanisms involved in this process.

Bb must adapt to dramatically different environments as it cycles from tick to vertebrate host, and understanding the genes involved in this process will enable the identification of key interactions to target to prevent transmission. When an infected tick feeds, *Bb* responds to bloodmeal-induced environmental changes and undergoes cellular modifications driven by key transcriptional circuits, including the RpoN-RpoS sigma factor cascade and the Hk1/Rrp1 two-component system (Radolf et al., 2012). *In vitro* analyses of *Bb* cells cultured in tick- or mammalian-like growth conditions have pointed to additional genetic determinants of tick-borne transmission by revealing widespread transcriptome remodeling during host switching (reviewed in Samuels et al., 2021). However, it is not fully clear how these *in vitro* expression changes correspond to complex *in vivo* changes over the course of a transmission bloodmeal, which comprises several physiologically distinct stages for the tick vector. Capturing comprehensive, longitudinal data on *Bb* gene expression from inside its vector has been hampered by technical challenges given the dynamic nature of the bloodmeal and the general low abundance of bacterial cells relative to the tick (Samuels et al., 2021). Although microarray approaches have been used to identify large scale changes in *Bb* gene expression between the first and second tick bloodmeals (Iyer et al., 2015),

we have limited temporal resolution into the molecular transitions that happen across key steps of tick feeding. This problem necessitates novel approaches to capture the transcriptomic changes of *Bb* within the natural tick environment.

While the full landscape of *Bb* transmission determinants is not yet known, we do have a growing knowledge of functional processes that are critical during the tick stage, such as motility, metabolism, and immune evasion (Kurokawa et al., 2020; Phelan et al., 2019). These functions often rely on the unique protein-rich *Bb* outer surface. Notably, several specific tick–*Bb* protein–protein interactions are important for *Bb* survival, migration, or transmission to the next host. *Bb* encodes an extensive outer surface protein (Osp) family with members that are differentially expressed during host switching. One of these proteins, OspA, binds a tick cell surface protein, tick receptor for OspA (TROSPA), which is required for successful *Bb* colonization of the tick midgut during the first acquisition bloodmeal (Pal et al., 2004). Several other proteins have also been linked to *Bb* migration within the tick (Pal et al., 2022). For example, BBE31 binds a tick protein TRE31, and disruption of this interaction decreases the number of *Bb* cells that successfully migrate from the tick gut to salivary glands (Zhang et al., 2011). However, these interactions alone are not sufficient to block *Bb* growth or migration in ticks, suggesting there are likely additional molecular factors from *Bb* and ticks at play during tick-borne transmission.

To provide a more comprehensive set of *Bb* determinants driving tick-borne transmission of this important human pathogen, we longitudinally mapped *Bb* genome-wide expression changes for bacterial cells isolated from inside ticks during the transmission bloodmeal. We developed a novel sequencing-based strategy for *ex vivo* transcriptomic profiling of *Bb* populations within feeding ticks. We identified 192 highly differentially expressed genes, including genes previously implicated in *Bb* transmission as well as many others. Genes upregulated during tick transmission were enriched for outer surface lipoproteins, suggesting *Bb* dramatically remodels its cell envelope as it migrates through the tick. Mass spectrometry analyses revealed dramatic changes in the tick environment over feeding, identifying new potential determinants of a more extensive and diverse set of tick–microbe molecular interactions than previously appreciated.

RESULTS

A two-step enrichment process facilitates robust transcriptional profiling of *Bb* during the tick bloodmeal

To gain a more comprehensive understanding of *Bb* gene expression throughout the tick phase of the transmission cycle, we developed an experimental approach to characterize the *Bb* transcriptome of spirochetes isolated from ticks during a bloodmeal. We aimed to establish a longitudinal transcriptional profile encompassing key pathogen transmission events each day of feeding after ticks attached to their mouse bloodmeal hosts (**Figure 1A**). The major bottleneck for such an RNA sequencing (RNA-seq) approach is capturing sufficient quantities of *Bb* transcripts from complex multi-organism samples in which pathogen transcripts represent a very small minority. Our initial attempts to uncover *Bb* mRNA by simply removing tick mRNA with polyA-depletion and removing tick rRNA sequences using Depletion of Abundant Sequences by Hybridization (DASH) (Dynerman et al., 2020; Gu et al., 2016) were unsuccessful. This approach resulted in an average of only 0.09% of RNA-seq reads mapping to *Bb* mRNA – approximately 10-fold less than we estimated would be needed to feasibly obtain robust transcriptome-wide gene expression analysis (Haas et al., 2012).

To dramatically increase *Bb* transcript representation in our libraries, we physically enriched *Bb* cells in tick lysates prior to library preparation by adding an initial step of immunomagnetic separation (**Figure 1B**). We took advantage of a commercial antibody previously generated against whole *Bb* cells (α*Bb*, RRID: AB_1016668). By western blot analysis, we confirmed that α*Bb* specifically recognized several *Bb* proteins, including surface protein OspA, which is highly prevalent on the *Bb* surface in ticks (**Figure S1A**). In addition, immunofluorescence microscopy with α*Bb* showed clear recognition of *Bb* cells from within the tick at each day of feeding (**Figure S1B**). After

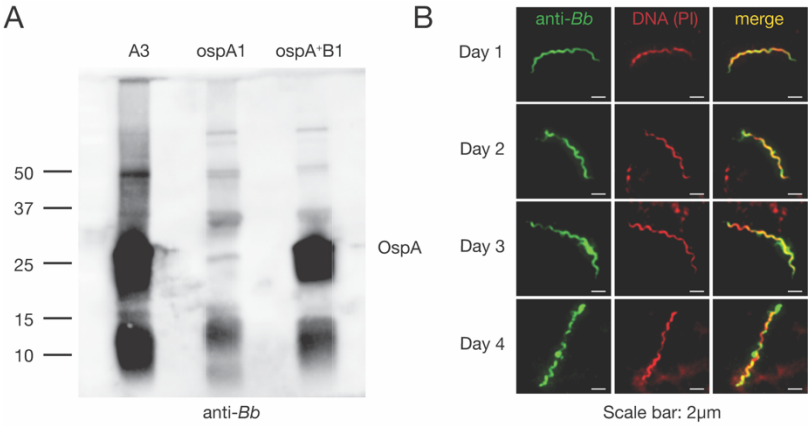

Figure S1. Anti-*Bb* antibody recognizes ospA and binds *Bb* in the tick throughout the bloodmeal. (**A**) Western blot with anti-*Bb* on lysate from cultured *Bb*: wildtype (A3, left), a mutant lacking ospA (ospA1), and the mutant with ospA restored (ospA+B1). Anti-*Bb* recognizes ospA among other proteins. (**B**) Immunofluorescence microscopy with anti-*Bb* (green) and propidium iodide (PI) (DNA, red) on each day of feeding (yellow is merge). Anti-*Bb* antibody recognizes *Bb* in the tick across the bloodmeal.

133 collecting infected ticks from mice one, two, three, and four days post-attachment, we used α*Bb*
134 and magnetic beads to enrich *Bb* cells away from the majority of the tick material in the lysates.
135 We tracked relative *Bb* enrichment through RT-qPCR of *Bb flaB* RNA and tick *gapdh* RNA in the

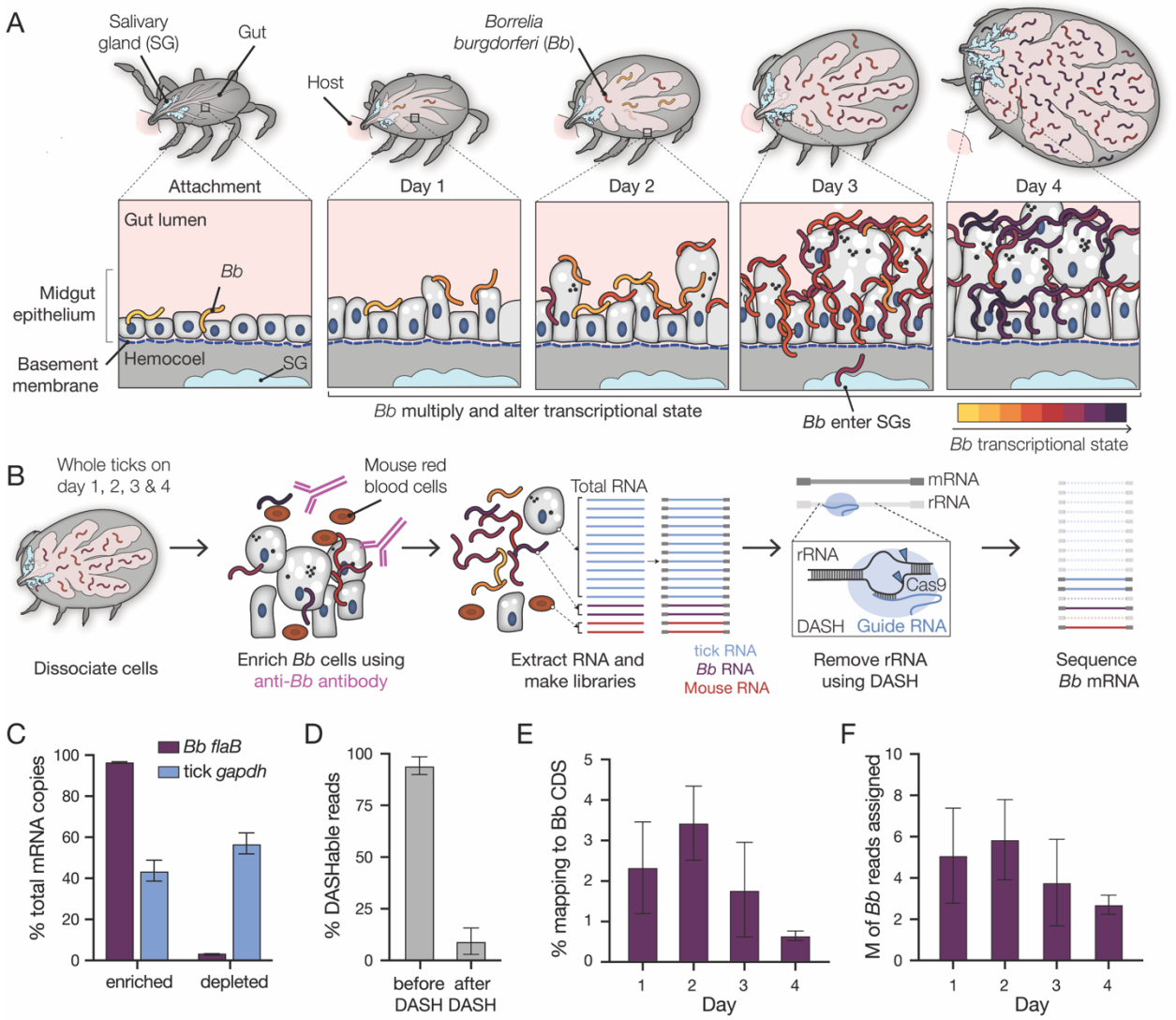

Figure 1. A two-step enrichment process facilitates robust transcriptional profiling of *Bb* during the tick bloodmeal. (**A**) Schematic of *Bb* during tick feeding. *Bb* in the nymphal tick midgut respond to the bloodmeal by multiplying and changing their transcriptional state. At the same time, the tick gut undergoes numerous changes to digest the bloodmeal. After two to three days of feeding, a small number of *Bb* leave the midgut and enter the salivary glands (blue), while the majority are left behind in the gut after engorgement. (**B**) Schematic of *Bb* enrichment process from feeding ticks. Whole ticks are dissociated, anti-*Bb* antibodies are added to lysates, and antibodies and *Bb* are captured magnetically. RNA is extracted and RNA-seq libraries are prepared. DASH is then used to remove rRNA before sequencing. This process increases *Bb* reads in the resulting sequencing. (**C**) RT-qPCR results showing the percentage of *Bb flaB* and tick *gapdh* RNA in the enriched versus depleted fractions after the enrichment process. Data come from 4 replicates each from day 2, day 3, and day 4, mean +/- SE. Nearly all *Bb flaB* RNA was found in the enriched fraction, while the majority of tick *gapdh* was found in the depleted fraction. (**D**) The percentage of reads mapping to rRNA before and after DASH. Data are shown as mean +/- SD. rRNA reads are drastically reduced after DASH. (**E**) The percentage of reads in RNA-seq libraries mapping to *Bb*. *Bb* mRNA reads make up a small but sufficient proportion of libraries for transcriptomics. Data are shown as mean +/- SD. (**F**) The number of reads in millions (M) mapped to *Bb* for each day. Data are shown as mean +/- SD. An average of 4.3 million reads per sample mapped to Bb genes, covering 92% of genes with at least 10 reads.

separated samples. Measuring *Bb flaB* RNA from both *Bb*-enriched samples and their matched *Bb*-depleted fractions, we found over 95% of total *Bb flaB* RNA was present in enriched fractions (**Figure 1C**), suggesting our approach captured the vast majority of *Bb* transcripts from the tick.

Total RNA recovered from the enrichment process was used to create RNA-seq libraries that subsequently underwent depletion of rRNA sequences from ticks, mouse, and *Bb* using DASH, which targets unwanted sequences for degradation by Cas9 (Gu et al., 2016; Ring et al., 2022). DASH reduced unwanted sequences from 94% to 9% of our total libraries, greatly increasing the relative abundance of *Bb* transcripts (**Figure 1D**). For resulting libraries generated across feeding (**Table S1**), between 0.6% and 3.4% of reads mapped to *Bb* coding regions (**Figure 1E**), which translated to an average of 4.3 million *Bb* reads per sample (**Figure 1F**). Read coverage was sufficient for downstream differential expression analyses for the vast majority of *Bb* genes, with at least 10 reads mapping to 92% of *Bb* genes. To evaluate whether our approach introduced any major artifacts, we sequenced and compared RNA-seq libraries from *in vitro* cultured *Bb* cells before and after immunomagnetic enrichment. We found minimal expression differences (29 genes with $p<0.05$, fold changes between 0.83-1.12) (**Figure S2, Table S2**), suggesting experimental enrichment did not significantly alter global transcriptome profiles for *Bb*. Thus, we developed an approach to enable genome-wide analysis of *Bb* population-level expression changes that occur within the feeding tick during transmission.

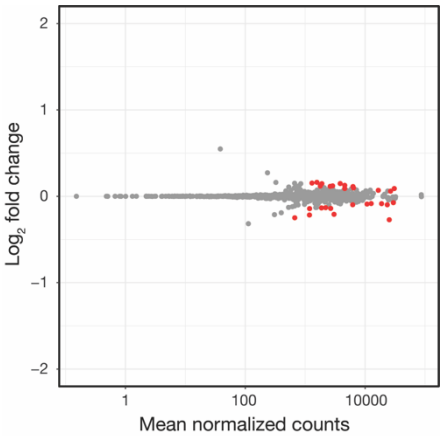

Figure S2. Enrichment process does not induce large scale gene expression changes in *in vitro* cultured *Bb*. Log_2 fold changes vs. mean normalized number of counts comparing cultured *Bb* input and samples after enrichment with anti-*Bb*. n=3. Red dots, p-value < 0.05, Wald tests. The gene expression changes induced during processing are much smaller than those observed between days of feeding.

Global *ex vivo* profiling of *Bb* reveals extent and kinetics of transcriptional changes

To provide a broad overview of *Bb* expression changes during feeding, we performed principal component analysis (PCA) on the *Bb* transcriptome data from one, two, three, and four days post-attachment (n=4). We reasoned that if many longitudinal expression changes were occurring across *Bb* populations, we would observe greater data variability between time points than between biological replicates. Indeed, we found replicates from each day grouped together, whereas distinct time points were largely non-overlapping. The first principal component, which

170 explained 64% of the variance in our data, correlated well with day of feeding (**Figure 2A**). The
171 global pattern suggested that *Bb* gene expression changes generally trended in the same
172 direction over the course of feeding with the most dramatic differences between flanking
173 timepoints on day 1 and day 4.
174
175 Using day 1 (early attachment) as a baseline, we performed differential expression analysis for
176 all *Bb* genes at subsequent time points and examined changes above a twofold threshold (**Figure**
177 **2B, Table S3**). These analyses mirrored the global longitudinal expression pattern predicted by
178 our PCA. The total number of differentially expressed (DE) genes increased steadily over time
179 and peaked at day 4, which when compared to day 1 had 186 DE genes, including 153
180 upregulated and 33 downregulated (**Figure 2C-E**). Across time points, DE genes were highly
181 overlapping and largely changed in the same directions. In all three comparisons, we found 192

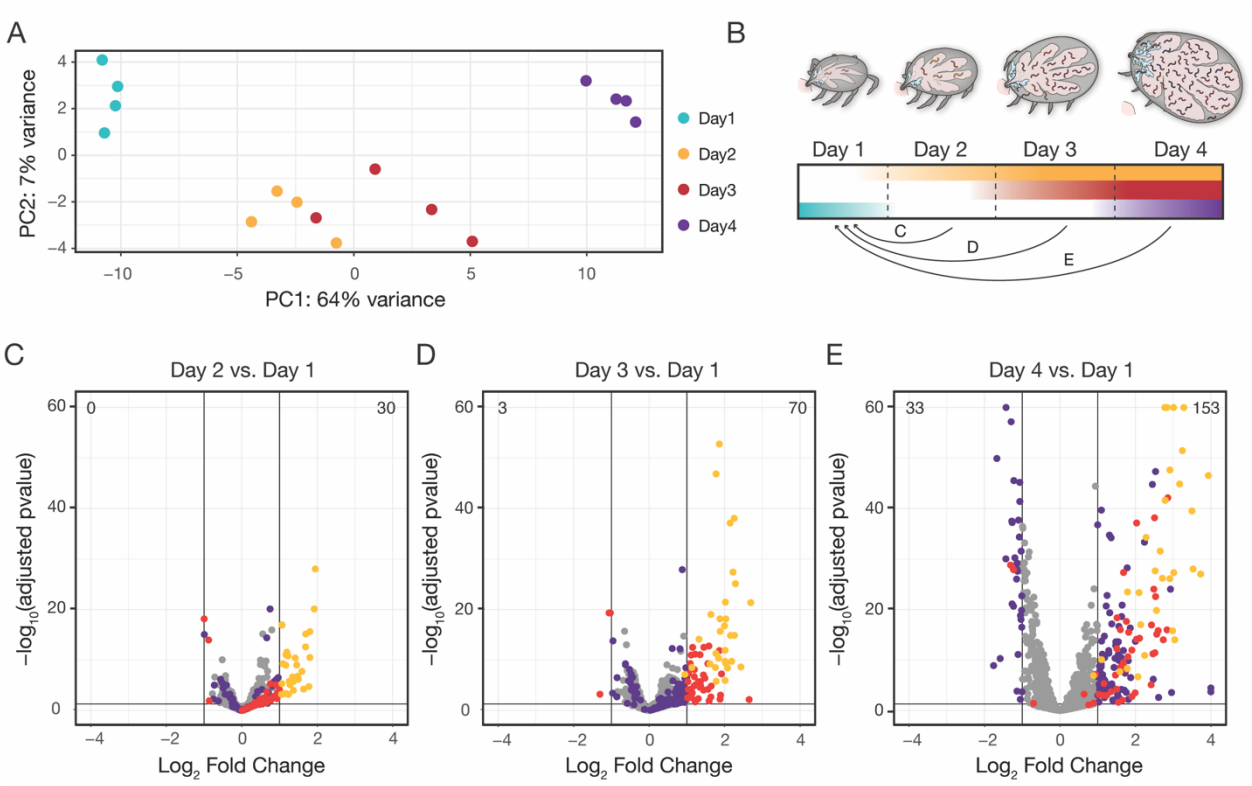

Figure 2. Global *ex vivo* profiling of *Bb* reveals extent and kinetics of transcriptional changes. (**A**) Principal component analysis of samples from across feeding. PC1 correlates strongly with day of feeding. (**B**) Schematic depicting how data was analyzed, as pairwise comparisons between the first day after attachment and all other days. (**C-E**) Volcano plots of differentially expressed genes of day 2 versus day 1 after attachment (**C**), day 3 versus day 1 (**D**), and day 4 versus day 1 (**E**). The total number of upregulated genes is shown in the top right and downregulated genes is shown in the top left. Yellow dots are genes that change expression between day 1 and day 2, red dots are genes that change expression between day 1 and day 3, and purple dots are genes that change expression between day 1 and day 4. Two genes with $\log_2$ fold changes >4 are shown at 4, and five genes with -$\log_{10}$(padj) >60 are shown at 60. Only genes with at least a 2-fold change are highlighted. p-value < 0.05, Wald tests. By day 4 of feeding, 153 genes are upregulated and 33 genes are downregulated from day 1 baseline levels.

182 DE genes in total (**Table S4**). However, there were some notable differences between genes,
183 such as the overall timing and kinetics of expression changes. Transcript levels for some DE
184 genes changed suddenly over the course of feeding, while others were more gradual. To our
185 knowledge, this is the first comprehensive report of global *Bb* expression changes within feeding
186 ticks.
187
188 To help assess the integrity of our dataset, we examined expression profiles for previously
189 characterized targets of major transcriptional programs activated at the onset of the bloodmeal:
190 the Hk1/Rrp1 two-component system and the RpoN/RpoS sigma factor cascade (Caimano et al.,
191 2019, 2015). Between day 1 and day 4, the majority of genes previously reported to be activated
192 or repressed by Rrp1 *in vitro* (Caimano et al., 2015) trended significantly in the expected direction
193 *ex vivo* (111/148 upregulated, 37/57 downregulated, p<0.05, Wald tests, **Figure S3A**). The
194 majority of the genes previously reported to be activated by RpoS in a mammalian context,
195 including canonical targets *ospC* and *dbpA*, were also significantly upregulated during tick feeding
196 (33/55, p<0.05, Wald tests) (**Figure S3B**), along with *rpoS* itself (**Figure S3C**), as expected
197 (Hübner et al., 2001). However, very few genes repressed by RpoS in mammals were similarly
198 repressed in ticks (2/33, p<0.05, Wald tests). These data support the hypothesis that while RpoS-

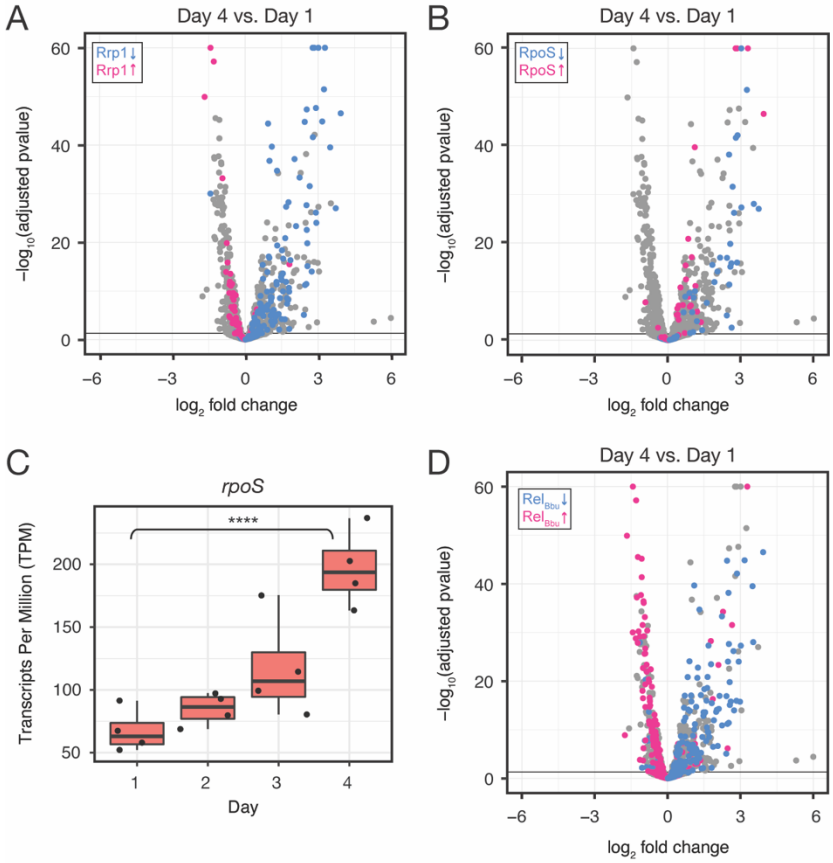

Figure S3. *Ex vivo* RNA-seq corroborates key transcriptional programs in the tick. (**A**) Volcano plot of DE genes comparing day 4 to day 1, with Rrp1-upregulated (blue) and downregulated (pink) genes. Rrp1-regulated genes correlate well with up and downregulated genes during feeding. (**B**) Volcano plot of DE genes comparing day 4 to day 1, with RpoS-upregulated (blue) and downregulated (pink) genes. Genes upregulated by RpoS in mammals increase during feeding, but genes repressed by RpoS in mammals are not repressed in the tick. (**C**) Tukey style boxplot of Transcripts Per Million (TPM) on each day for *rpo*S. Black dots represent replicates. ****p-value < 0.00001, Wald test. *rpoS* expression increases over the course of feeding. (**D**) Volcano plot of DE genes comparing day 4 to day 1, with Rel_{Bbu}-upregulated (blue) and downregulated (pink) genes. About half of Rel_{Bbu} genes change in the expected direction over feeding.

199 dependent gene activation occurs across both vertebrate and vector stages of *Bb* transmission,
200 RpoS-dependent repression is specific to spirochetes infecting a mammalian host (Caimano et
201 al., 2019, 2007). We also compared our DE genes to those regulated by Rel_{Bbu} as part of the
202 stringent response, another major transcriptional program active in *Bb* in the tick during nutrient
203 starvation (Drecktrah et al., 2015). About half of Rel_{Bbu}-regulated genes changed in the direction
204 expected if the stringent response was active during this time (**Figure S3D**); however, more of
205 the genes that were downregulated over feeding have been reported to be regulated by Rel_{Bbu}
206 than either RpoS or Rrp1, suggesting it may play some role during feeding.
207
208 By looking at these previously reported transcriptional regulons in our data, we were able to verify
209 that our data captured expected transcriptional programs active during tick feeding. Nevertheless,
210 25% of the twofold DE genes were not previously identified through these RNA-seq studies as
211 dependent upon RpoS, Rrp1, or Rel_{Bbu} (Caimano et al., 2019, 2015; Drecktrah et al., 2015), which
212 are the three main *Bb* regulatory programs active in the tick (Samuels et al., 2021). These
213 additional genes highlight the necessity of measuring transcription in the tick environment and
214 suggest we uncovered gene expression changes specific to the tick-stage of the *Bb* enzootic
215 cycle. The nature and dynamics of these changes provide insights into potential genetic
216 determinants of *Bb* survival, proliferation, and dissemination in the tick during transmission.
217
218 ***Bb* genes upregulated during feeding are found predominantly on plasmids**
219
220 *Bb* has a complex, highly fragmented genome (Barbour, 1988) (**Figure 3A**), including numerous
221 plasmids that are necessary during specific stages of the enzootic cycle (reviewed in Schwartz et
222 al., 2021) suggesting they contain genes that are crucial for pathogen transmission and survival.
223 In fact, many genes found on the plasmids have been previously shown to alter expression upon
224 environmental changes or in different host environments (Iyer et al., 2015; Ojaimi et al., 2005;
225 Revel et al., 2002; Tokarz et al., 2004). Thus, we reasoned that many of the 192 *Bb* genes that
226 change expression over the course of the tick bloodmeal would reside on the plasmids, and we
227 examined their distribution throughout the genome. Consistent with these previous reports, we
228 found that most of the upregulated genes were located on the plasmids (143/158; 90%), while
229 fewer were found on the chromosome (15/158; 10%) (**Figure 3B**), which is home to the majority
230 of metabolic and other housekeeping genes. In contrast, the majority of the downregulated genes
231 were found on the chromosome (27/34, 79%) (**Fig 3C**).
232

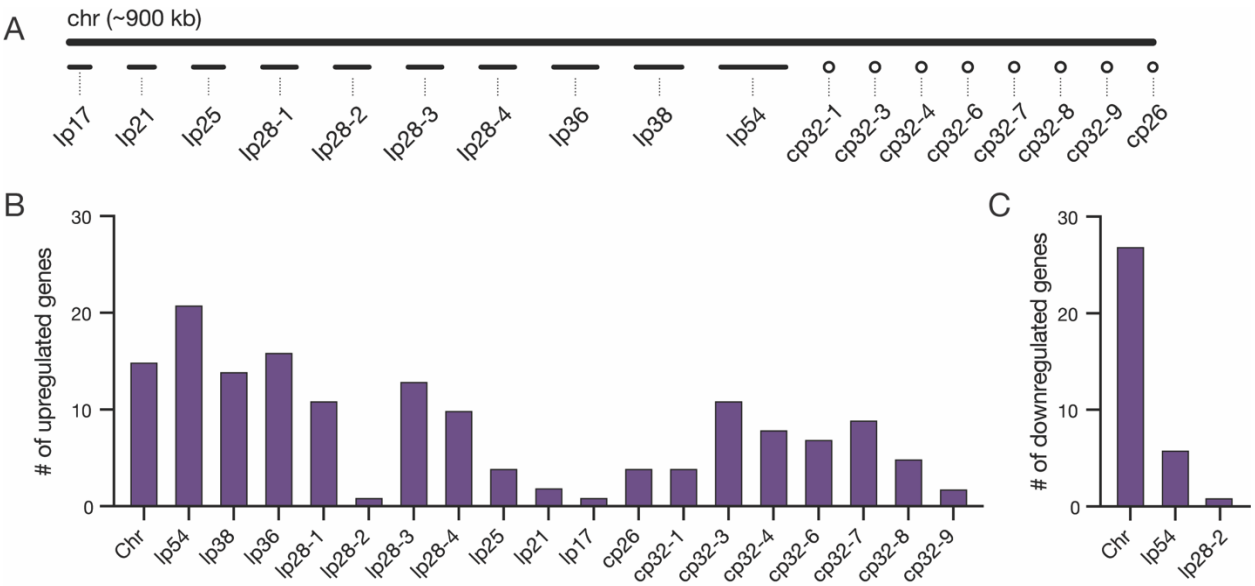

Figure 3. *Bb* genes upregulated during feeding are found predominantly on plasmids. (**A**) Schematic of the chromosome and plasmids in the *Bb* B31-S9 genome. (**B-C**) The number of genes from each chromosome or plasmid that increased (**B**) or decreased expression (**C**) twofold during feeding. Upregulated genes are distributed across plasmids, while downregulated genes are found on the chromosome and lp54.

233 Several plasmid-encoded genes that were longitudinally upregulated in our datasets have known
234 roles during the tick bloodmeal or in mammalian infection. For example, linear plasmid 54 (lp54),
235 which is an essential plasmid present in all *Bb* isolates (Casjens et al., 2012), contained the largest
236 number of upregulated genes. Many of the genes on lp54 are known to be regulated by RpoS
237 during feeding, including those encoding adhesins DbpA and DbpB, which are important for
238 infectivity in the host (Blevins et al., 2008). This set also included five members of a paralogous
239 family of outer surface lipoproteins BBA64, BBA65, BBA66, BBA71, and BBA73. BBA64 and
240 BBA66 are necessary for optimal transmission via the tick bite (Gilmore et al., 2010; Patton et al.,
241 2013). These findings indicate our dataset captures key *Bb* transcriptional responses known to
242 be important for survival inside the tick during a bloodmeal.
243
244 Many upregulated genes were encoded by cp32 plasmid prophages. *Bb* strain B31-S9 harbors
245 seven cp32 isoforms that are highly similar to each other (Casjens et al., 2012). When cp32
246 prophages are induced, phage virions called ϕBB1 are produced (Eggers and Samuels, 1999). In
247 addition to phage structural genes, cp32 contain loci that encode various families of paralogous
248 outer surface proteins (Stevenson et al., 2000). Amongst the cp32 genes that increased over
249 feeding were members of the RevA, Erp, and Mlp families, which are known to increase
250 expression during the bloodmeal (Gilmore et al., 2001). We also found several phage genes that
251 were upregulated, including those encoding proteins annotated as phage terminases on cp32-3,
252 cp32-4, and cp32-7 (BBS45, BBR45, and BBO44). Some cp32 genes have been shown to

253 change expression in response to temperature changes (Tokarz et al., 2004) and as a part of the
254 stringent response regulated by Rel_{Bbu} (Drecktrah et al., 2015). Our data suggest that some
255 prophage genes are upregulated over the course of tick feeding, raising the possibility that cp32
256 prophage are induced towards the end of feeding. Overall, our data support the long-held idea
257 that the *Bb* plasmids, which house many genes encoding cell envelope proteins, proteins of
258 unknown function, and prophage genes, play a critical role in the enzootic cycle during the key
259 transition period of tick feeding.
260
261 ***Bb* genes encoding outer surface proteins are enriched among upregulated genes**
262
263 To gain a better overall sense of the types of genes that changed over feeding and the timing of
264 those changes, we grouped DE genes into functional categories. Since a high proportion of
265 plasmid genes encode lipoproteins within the unique protein-rich outer surface of *Bb*, genes of
266 unknown function, and predicted prophage genes (Casjens et al., 2000; Fraser et al., 1997), we
267 expected that many of the DE genes would fall into these categories. We classified the genes as
268 related to either: cell envelope, bacteriophage, cell division, DNA replication and repair,
269 chemotaxis and motility, metabolism, transporter proteins, transcription, translation, stress
270 response, protein degradation, or unknown (as in Drecktrah et al., 2015)(see **Table S4**).
271
272 Of the genes that increased at least twofold over feeding, the clear majority each day of feeding
273 fell into two broad categories, cell envelope (55 of 158 total genes) and proteins of unknown
274 function (69 of 158 total genes), with fewer genes related to metabolism, chemotaxis and motility,
275 transporters, bacteriophage, cell division, and transcription (**Figure 4A**). In contrast to the
276 upregulated genes, genes downregulated during feeding were more evenly distributed among the
277 functional categories – including translation, protein degradation, transcription, and metabolism –
278 consistent with many of them being located on the chromosome.
279
280 When looking at changes across these functional categories, the overrepresentation of cell
281 envelope proteins was striking, while not unexpected. The *Bb* outer surface is covered with
282 lipoproteins (**Figure 4B**), and these proteins are critical determinants in *Bb* interactions with the
283 various environments encountered during the enzootic cycle (Kurokawa et al., 2020). We found
284 that more than half of these outer surface lipoproteins changed expression during this time, with
285 46 of 83 total outer surface lipoproteins (Dowdell et al., 2017) differentially expressed twofold over

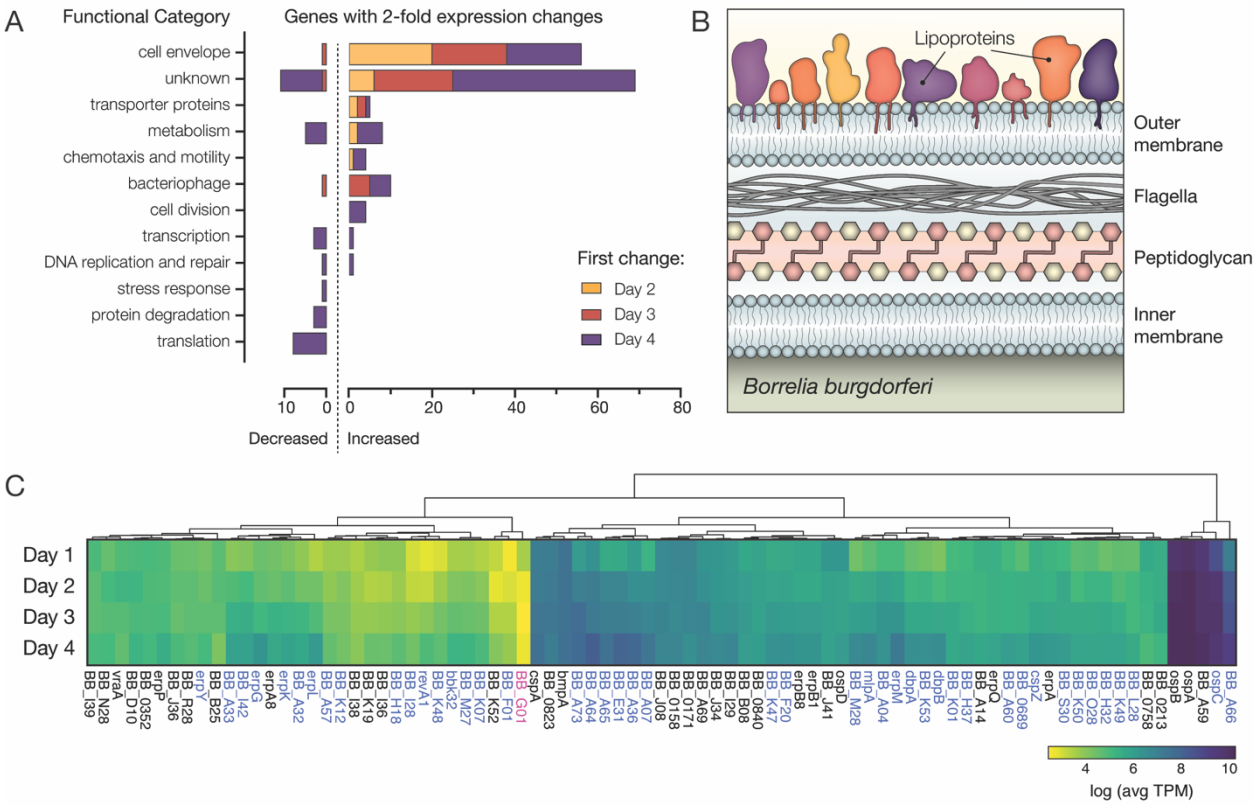

Figure 4. *Bb* genes encoding outer surface proteins are enriched among upregulated genes. (**A**) The number of *Bb* genes that change over the course of tick feeding sorted into functional categories. Genes that first change 2 days after attachment are shown in yellow, 3 days after attachment in red, and 4 days after attachment in purple. A majority of upregulated genes fall into cell envelope and unknown categories. (**B**) Schematic of the outer membrane of *Bb* showing the location of outer surface lipoproteins. (**C**) Heat map of the average Transcripts Per Million (TPM) of all genes encoding outer surface lipoproteins across the 4 days of tick feeding. Genes in blue were twofold upregulated and genes in pink twofold downregulated over feeding. A majority of genes encoding outer surface proteins increased in expression throughout feeding, while having different magnitudes of expression.

feeding (**Figure 4C**). These data suggested widespread changes may be occurring on the *Bb* outer surface during feeding.

To understand the functional implications of expression changes in a majority of outer surface lipoproteins, we also compared their relative expression. The magnitude of expression varied greatly, with *ospA*, *ospB*, *ospC*, and *bba59* being the most highly expressed outer surface protein transcripts. Many of the outer surface protein genes that we found increased expression over feeding were much less abundantly expressed (**Table S5**). However, even the genes that appeared to have low expression in these population level measurements could play important roles in transmission if they are highly expressed in a small number of crucial cells, such as those that ultimately escape the midgut. While bulk RNA-seq cannot distinguish what is happening at the single cell level, our data suggest that during the bloodmeal, *Bb* are undergoing a complex

298 outer surface transformation driven by increases in a majority of the genes encoding these crucial
299 lipoproteins.
300
301 **Identification of candidate tick interaction partners of *Bb* cells *ex vivo***
302
303 Our RNA-seq data suggested that the outer surface of *Bb* transforms over the course of feeding
304 as *Bb* are primed for transmission to a vertebrate host. At the same time, the tick midgut
305 environment is changing as the tick begins to digest its bloodmeal. Tick-*Bb* interactions are likely
306 crucial at the beginning of the tick bloodmeal, as *Bb* adhere to the tick gut epithelium before
307 becoming motile and migrating out of the midgut and into the salivary glands (Dunham-Ems et
308 al., 2009). Some *Bb* outer surface proteins, such as BBE31 and BBA52 play key roles in pathogen
309 migration through interactions with the tick environment (Kurokawa et al., 2020). We wanted to
310 explore the changing tick environment to identify tick proteins with which *Bb* could interact
311 throughout the tick bloodmeal. Since our *Bb* enrichment process retained some tick material, we
312 reasoned that tick proteins that interact with *Bb* would be present in these samples.
313
314 To outline the changes occurring in the tick during feeding and to identify candidate *Bb*-interacting
315 tick proteins, we used mass spectrometry to survey the content of the tick material that was

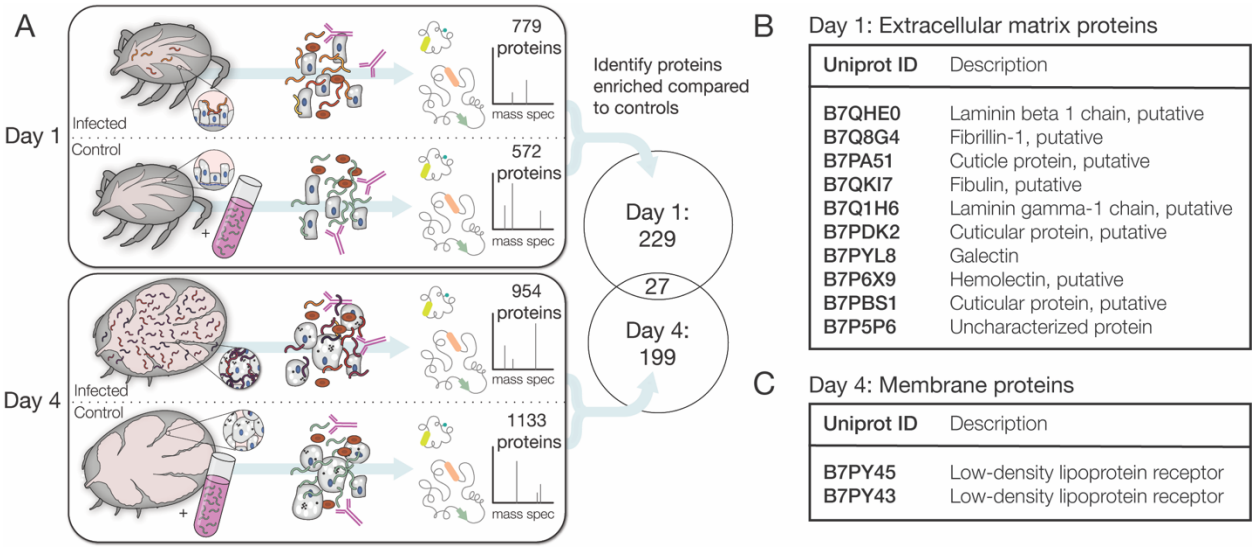

Uniprot ID	Description
B7QHE0	Laminin beta 1 chain, putative
B7Q8G4	Fibrillin-1, putative
B7PA51	Cuticle protein, putative
B7QKI7	Fibulin, putative
B7Q1H6	Laminin gamma-1 chain, putative
B7PDK2	Cuticular protein, putative
B7PYL8	Galectin
B7P6X9	Hemolectin, putative
B7PBS1	Cuticular protein, putative
B7P5P6	Uncharacterized protein

Uniprot ID	Description
B7PY45	Low-density lipoprotein receptor
B7PY43	Low-density lipoprotein receptor

Figure 5. Identification of candidate tick interaction partners of *Bb* cells *ex vivo*. (**A**) Schematic of experiment to determine candidate tick proteins interacting with *Bb* over the course of feeding. Ticks were collected 1 day after attachment and 4 days after attachment. Uninfected ticks at the same time points were mixed with cultured *Bb* as controls. *Bb* was enriched with anti-*Bb* antibody as in RNA-seq experiments and then subjected to mass spectrometry to identify tick proteins present in the samples. Venn diagram depicts the proteins enriched in day 1 and day 4 samples over controls. Tick proteins that are enriched with *Bb* vary greatly over the course of feeding. (**B**) Tick proteins uniquely identified one day after attachment that are annotated as extracellular matrix (ECM) proteins. (**C**) Tick proteins uniquely identified four days after attachment that are annotated as low-density lipoprotein receptors. ECM and membrane proteins may be good candidates for *Bb*-interacting proteins.

316 enriched along with the *Bb* cells we sequenced at early and late stages during feeding. We purified
317 proteins from the α*Bb*-enriched fraction of crushed infected ticks on day 1 after attachment and
318 day 4 after attachment in triplicate. As controls for each day, we also performed the *Bb* enrichment
319 process on lysate from uninfected ticks mixed with *in vitro* cultured *Bb* to help rule out proteins
320 that were not pulled down through *in vivo* tick-*Bb* interactions (**Figure 5A**). We identified between
321 414 and 2240 protein groups per sample replicate. To identify proteins of interest, we looked for
322 those that were detected in at least two of three replicates with infected ticks and had a mean
323 average coverage twice that of uninfected ticks mixed with cultured *Bb*. We found 256 proteins
324 that were enriched with *Bb* from infected ticks one day after attachment and 226 proteins that
325 were enriched with *Bb* from infected ticks four days after attachment (**Table S6**). Of these proteins,
326 only 27 were detectable on both days, suggesting the tick proteins present upon *Bb* enrichment
327 change dramatically over the course of feeding. The vast majority of all detected proteins were
328 from ticks (98%). Amongst the small number of *Bb* proteins, we identified OspC in the samples
329 from day 4 after attachment but not day 1 after attachment, confirming the expression change we
330 saw in our RNA-seq. The distinct sets of tick proteins we identified at each timepoint suggest
331 dramatic changes occur in the *Bb*-infected tick midgut environment during feeding that may alter
332 the landscape of tick-*Bb* interactions.
333
334 Some of the proteins enriched with *Bb* from the tick may be good candidates for key *Bb*-interacting
335 partners during feeding, especially if they are localized to the surface of tick cells where they may
336 encounter *Bb*. The scarcity of both predicted and experimentally validated functions and
337 localizations for tick proteins makes it difficult to fully assess the potential for tick protein
338 interactions with extracellular *Bb*. Nevertheless, of the proteins found exclusively one day after
339 attachment, 10 were categorized as extracellular matrix proteins using the PANTHER gene
340 database (Thomas et al., 2022), and this category was statistically enriched (Fisher's exact test,
341 FDR=0.000093) (**Figure 5B, Table S7**). 30 additional proteins were annotated with a cellular
342 component as plasma membrane. Four days after attachment, we did not detect any annotated
343 extracellular matrix proteins; however, we identified 31 proteins that are likely to be found at the
344 membrane, including two proteins annotated as putative low-density lipoprotein receptors (**Figure
345 5C, Table S8**). These extracellular matrix and membrane proteins may be the most likely to
346 directly interact with *Bb* during this timeframe and are candidates for tick proteins important in the
347 *Bb* dissemination process. The proteins present in the changing tick environment may be key
348 determinants of pathogen transmission as *Bb* remodels its outer surface while preparing to
349 migrate through the tick to a new host.

350 **DISCUSSION**

351 Vector-borne pathogens must adapt to distinct environments as they are transmitted by
352 arthropods to colonize new bloodmeal hosts. The tick-borne Lyme disease pathogen *Bb*
353 undergoes transcriptional changes inside its vector over the course of a single bloodmeal that are
354 important for a number of key transmission events. For example, expression changes enable
355 survival in the feeding tick (He et al., 2011), facilitate transmission across several internal
356 compartments into the bloodmeal host (Kurokawa et al., 2020), and prime bacteria for successful
357 infection of the next host (Kasumba et al., 2016). Capturing these changes as they occur *in vivo*
358 has been challenging due to the low relative abundance of *Bb* material inside of the rapidly
359 growing, blood-filled tick. To date, many advances in our understanding of *Bb* expression during
360 transmission have come from tracking changes in small subsets of genes during tick feeding
361 (Gilmore et al., 2001), leveraging *Bb* culture conditions that approximate environmental changes
362 across its lifecycle (Ojaimi et al., 2005; Revel et al., 2002; Tokarz et al., 2004), and defining
363 transcriptional regulons outside of the tick (Caimano et al., 2019, 2015; Drecktrah et al., 2015).
364 Here, we developed an experimental RNA-seq-based strategy to more directly and longitudinally
365 profile gene expression for *Bb* populations isolated from ticks over the course of a transmitting
366 bloodmeal.

367

368 Our longitudinal collection of transcriptomes for *Bb* cells isolated from ticks serves as a resource
369 and starting point for delineating the functional determinants of *Bb* adaptation and transmission.
370 Our transcriptome profiles reveal more extensive expression changes for *Bb* outer surface
371 proteins than previously appreciated. These results raise the possibility that *Bb* is actively
372 remodeling its outer coat to navigate the dynamic tick environment during feeding, akin to
373 wardrobe changes across seasons. These outer surface changes may play roles in the
374 persistence of *Bb* in the tick, cell adhesion, or in immune evasion, either inside of the tick or later
375 in the vertebrate host (Kenedy et al., 2012). It has long been observed that molecular interactions
376 between pathogens and the midgut of their vectors are key determinants of transmission (Barillas-
377 Mury et al., 2022). Modifications to the *Bb* surface could facilitate different tick–pathogen
378 interactions that are critical for its physical movement through tick compartments. Notably, we
379 also identified numerous genes of unknown function that change expression during feeding.
380 Although challenging to address, efforts focused on uncovering the contribution of these genes
381 to the *Bb* life cycle could be groundbreaking for understanding the unique aspects of tick-borne
382 transmission.

383

More comprehensive knowledge about *Bb* outer surface proteins and their functional consequences could lead to new avenues for curtailing the spread of Lyme disease. Protective vaccines against vector-borne pathogens have often targeted surface proteins encoded by pathogens (Kovacs-Simon et al., 2010). While previous Lyme disease vaccine efforts effectively targeted the highly expressed *Bb* outer surface protein OspA (Steere et al., 1998), more targets could increase the likelihood of a successful vaccine. Our study provides a catalog of new *Bb* candidates that could be explored. In addition, our biochemical pull-downs using tick-isolated *Bb* cells as bait unearthed a preliminary list of potential tick proteins that could be involved in tick–*Bb* molecular interactions. Blocking molecular interactions that are functionally critical for transmission could also be explored as a therapeutic strategy (Barillas-Mury et al., 2022; Manning and Cantaert, 2019).

Our transcriptomic resource provides critical insights into *Bb* population-level changes during the vector stage of its lifecycle, an important starting point for understanding the primary drivers of tick-borne transmission. Strikingly few *Bb* cells out of the total pathogen population in ticks are ultimately transmitted to the next host during feeding. There are several major bottlenecks to infection, including dissemination to the tick salivary glands and survival upon inoculation of the host (Dunham-Ems et al., 2009; Rego et al., 2014). There may be important physiological or molecular variations across *Bb* cells within the population residing in the tick that contribute to these differential outcomes. An important clue is the fact that *Bb* proteins are indeed heterogeneously expressed across cells within the feeding tick midgut (Ohnishi et al., 2001). Conducting transcriptomic analyses at the single-cell level will be key. Given that only a small number of *Bb* escape the tick midgut, genes that appear unaltered or show low expression levels across the bulk population could still play an outsized role in infection for a minority of the cells. Our work provides a foundational methodology that can be leveraged to greatly improve the resolution of tick–microbe studies. Technological advances stemming from this work will provide molecular details that potentiate new questions and may unearth surprising mechanistic insights into the unique lifestyles of tick-borne pathogens.

413 **METHODS**

414 ***B. burgdorferi* culture**

415 *Bb* strain B31-S9 (Rego et al., 2011) was provided by Dr. Patricia Rosa (NIAID, NIH, RML) and
416 cultured in BSK II media at 35°C, 2.5% CO_2.

417

418 **Tick feeding experiments**

419 *I. scapularis* larvae were purchased from the Tick Lab at Oklahoma State University (OSU) (for
420 RNA-seq experiments) or provided by BEI Resources, a division of the Center for Disease Control
421 (for mass spectrometry experiments). Before and after feeding, ticks were maintained in glass
422 jars with a relative humidity of 95% (saturated solution of potassium nitrate) in a sealed incubator
423 at 22°C with a light cycle of 16h/8h (light/dark). Animal experiments were conducted in
424 accordance with the approval of the Institutional Animal Care and Use Committee (IACUC) at
425 UCSF. Ticks were fed on young (4–6-week-old) female C3H/HeJ mice acquired from Jackson
426 Laboratories. Mice were anesthetized with ketamine/xylazine before placement of ≤ 100 larval or
427 ≤ 30 nymphal ticks. Ticks were either pulled off isoflurane anesthetized mice at various times
428 during feeding (1-3 days after placement) or allowed to feed to repletion and collected from mouse
429 cages. Replete larval ticks were placed in the incubator to molt before being used as nymphs in
430 experiments.

431

432 **Western blot with anti-*Bb* antibody**

433 To determine whether the anti-*Bb* antibody targeted ospA, we cultured wildtype *Bb* (B31-A3),
434 ospA1-mutants (ospA1) and ospA-restored *Bb* ($ospA^{+}B1$) (Battisti et al., 2008) to approximately
435 $5x10^{7}$ *Bb*/mL and centrifuged 3 mLs of culture for 7 minutes at 8000 x g, washing twice with PBS.
436 Pelleted cells were lysed in 50 µL of water, and 25 ng per sample was mixed with 5X loading dye
437 (0.25% Bromophenol Blue, 50% Glycerol, 10% Sodium Dodecyl Sulfate, 0.25M Tris-Cl pH 6.8,
438 10% B-Mercaptoethanol), run on a Mini-PROTEAN TGX 4-15% gel (Biorad), and transferred
439 using the Trans-Blot Turbo Transfer System (Biorad). After transfer, the blot was blocked for 30
440 minutes at 4°C in TBST (Tris buffered saline with .1% tween) with 5% milk, then treated with anti-
441 *Bb* antibody (Invitrogen: PA1-73004; RRID: AB_1016668) diluted 1:10,000 for 1 hour at room
442 temperature, followed by anti-rabbit HRP secondary antibody (Advansta) diluted 1:5,000 for 45
443 minutes at room temperature with short PBST washes between each step. Blots were exposed
444 using Clarity Western ECL Substrate (Biorad) and imaged using the Azure C400 imaging system
445 (Azure Biosystems). This experiment was repeated three times.

446

447 **Enrichment of *Bb* from feeding ticks**

448 To sequence RNA from *Bb* from feeding ticks, we enriched *Bb* to increase the ratio of *Bb* to tick
449 material. Larval ticks were fed to repletion on three mice that were infected with *Bb* through
450 intraperitoneal and subcutaneous injection with 10^4 total *Bb*. Approximately five months later, the
451 molted nymphal ticks were fed on eight mice. We estimated that 83% of the ticks were infected
452 with *Bb* by crushing 12 unfed nymphs in BSK II media and checking for viable *Bb* days later. Ticks
453 were pulled from all mice and pooled into four replicates 1 day after placement (14 ticks per
454 replicate), 2 days after placement (12 ticks per replicate), and 3 days after placement (6 ticks per
455 replicate) and collected from cages 4 days after placement (7 ticks per replicate). Shortly after
456 collection, ticks were washed with water and placed in a 2 mL glass dounce grinder (Kimble) in
457 500 µL of phosphate-buffered saline (PBS). Ticks were homogenized first with the large clearance
458 pestle and then the small clearance pestle. The homogenate was transferred to a 1.5 mL
459 Eppendorf tube and 500 µL of PBS was added to total 1 mL. At this stage, 50 µL of homogenate
460 was removed as an input sample and mixed with 500 µL of TRIzol (Invitrogen) for RNA extraction.
461 2 µL of anti-*Bb* antibody (Invitrogen: PA1-73004; RRID: AB_1016668) was added to the
462 homogenate, which was then placed on a nutator at 4°C for 30 minutes. During incubation, 50 µL
463 of Dynabeads Protein G (Invitrogen) per sample were washed twice in PBS. After incubation with
464 the antibody, the homogenate and antibody mixture were added to the beads. This mixture was
465 placed on a nutator at 4°C for 30 minutes. Tubes were then placed on a magnet to secure beads,
466 and the homogenate was removed and saved to create depleted samples. The depleted
467 homogenate was centrifuged at 8,000 x g for 7 minutes, 900 µL of supernatant was removed, and
468 500 µL of TRIzol was added to the pellet to create depleted samples. The beads were washed
469 twice with 1 mL of PBS, resuspending the beads each time. The second wash was removed and
470 500 µL of TRIzol was added to the beads to create enriched samples. RNA was extracted from
471 all input, enriched, and depleted samples using the Zymo Direct-zol RNA Microprep Kit with on-
472 column DNase treatment (Zymo Research). The step-by-step *Bb* enrichment protocol is available
473 at: dx.doi.org/10.17504/protocols.io.36wgqjrbovk5/v1.

474

475 **Enrichment of *Bb* from culture**

476 To test whether the *Bb* enrichment process altered gene expression levels, we performed the
477 enrichment protocol on cultured *Bb*. We grew three tubes of *Bb* in BSK II media to $9x10^4$ *Bb*/mL
478 at 35°C. 1 mL of culture was spun down at 8,000 x g for 7 minutes, media was removed, *Bb* were
479 washed in 1 mL of PBS and spun again. Pelleted *Bb* were resuspended in 1 mL of fresh PBS.
480 These samples were used as starting homogenate for the *Bb* enrichment protocol and input,

481 enriched, and depleted fractions were collected as above. RNA-seq libraries from these samples
482 were prepared and sequenced as below.
483
484 **RNA-seq library preparation and sequencing**
485 To make RNA-seq libraries from enriched *Bb* RNA, we used 50 ng of total RNA as input into the
486 NEBNext Ultra II Directional RNA Library Prep Kit for Illumina (New England BioLabs). We
487 prepared libraries following the manufacturer's protocol for use of the kit with purified mRNA or
488 rRNA-depleted RNA, despite starting with total RNA. Libraries were barcoded using NEBNext
489 Multiplex Oligos for Illumina Dual Index (New England BioLabs).
490
491 To deplete reads from the libraries that were from tick, *Bb*, or mouse rRNA, we used Depletion of
492 Abundant Sequences by Hybridization (DASH) (Gu et al., 2016), which targets Cas9 to unwanted
493 reads in RNA-seq libraries using custom dual-guide RNAs (dgRNAs). Our dgRNAs targeted short
494 sequences within tick rRNA, mouse rRNA, and *Bb* rRNA that were designed using DASHit
495 software (Dynerman et al., 2020). We ordered crRNAs that targeted our sequences of interest
496 (Ring et al., 2022). To transcribe the dgRNAs, we followed our protocol for In Vitro Transcription
497 for dgRNA V2 (Lyden et al., 2019b). Both tracrRNA and pooled crRNA DNA templates were
498 annealed to equimolar amounts of T7 primer by heating to 95°C for 2 minutes and slowly cooling
499 to room temperature. Annealed templates were used in 1 mL in vitro transcription reactions with:
500 120 µL10X T7 buffer (400 mM Tris pH 7.9, 200 mM MgCl2, 50 mM DTT, 20 mM spermidine
501 (Sigma)), 100 µL of T7 enzyme (custom prepped enzyme from E. Crawford, diluted 1:100 in T7
502 buffer, final concentration: 100 µg/mL), 300 µl NTPs (25 mM each, Thermo Fisher Scientific), 4
503 µg of annealed crRNA template or 8 µg of annealed tracrRNA template, and water to 1 mL. In
504 vitro transcription was performed for 2 hours at 37°C. Reactions were purified twice with the Zymo
505 RNA Clean & Concentrator-5 Kit (Zymo Research). To form the dgRNA complex for DASH, crRNA
506 and tracrRNAs were diluted to 80 µM, mixed in equimolar amounts and annealed by heating to
507 95ºC for 30 seconds and cooling slowly to room temperature.

508 After transcription of dgRNAs, we performed DASH Protocol Version 4 (Lyden et al., 2019a) on
509 each library individually. Cas9 and transcribed dgRNAs were prepped by mixing: 2.5 µL 10X Cas9
510 buffer, 5 µL Cas9 (New England BioLabs), and 5 µL of 40 µM transcribed dgRNAs. The mixture
511 was incubated at 37°C for 5 minutes before 7.5 µL of RNA-seq library (2.8 nM) was added. The
512 mixture was incubated at 37°C for 1 hour and then purified with Zymo DNA Clean & Concentrator-
513 5 (Zymo Research) following the PCR product protocol and eluting DNA into 10.5 µL of water.

514 During cleanup, Cas9 was again mixed with buffer and dgRNAs and incubated at 37°C for 5
515 minutes. Following cleanup, eluted DNA was added to the second Cas9-dgRNA mixture and
516 incubated at 37°C for 1 hour for a second time. Then, 1 µL of proteinase K (New England Biolabs)
517 was added, and the mixture was incubated at 50°C for 15 min. The libraries were then purified
518 with 0.9x volume of sparQ PureMag Beads (QuantaBio) following the standard protocol, eluting
519 in 24 µL of water. rRNA-depleted RNA-seq libraries were then amplified in a BioRad CFX96 using
520 the Kapa HiFi Real-Time Amplification Kit in a 50 µL reaction with 25 µL master mix, 23 µL of the
521 DASHed library pool, and 2 µL of 25 µM mix of Illumina P5 (5'-
522 AATGATACGGCGACCACCGAGATCT) and P7 (5'- CAAGCAGAAGACGGCATACGAGAT)
523 primers. The qPCR program for amplification was as follows: 98°C for 45 sec (1 cycle), (98°C for
524 15 sec, 63°C for 30 sec, 72°C for 45 sec, plate read, 72°C for 20 sec) for 10 cycles (day 3 and
525 day 4 samples) or 11 cycles (day 1 and day 2 samples). The libraries were removed from cycling
526 conditions before leaving the exponential phase of amplification and then purified with 0.9X
527 volume of sparQ PureMag Beads according to the standard protocol.

528 Following DASH, RNA-seq libraries were sequenced on an Illumina NovaSeq S2 (2 lanes) with
529 paired-end 100 base pair reads. Libraries from *in vitro* cultured control experiment were
530 sequenced on an Illumina NextSeq with paired-end 75 base pair reads. FASTQ files and raw *Bb*
531 read counts for *in vitro* control experiment (GSE217146) and *ex vivo* experiment (GSE216261)
532 have been deposited in NCBI's Gene Expression Omnibus (Edgar et al., 2002) under SuperSeries
533 accession number GSE217236.

534 **RNA-seq data analysis**

535 To measure the success of our rRNA depletion through DASH, we used DASHit software
536 (Dynerman et al., 2020) to determine the percentage of reads that would be DASHable by our
537 guide RNAs (Ring et al., 2022). For pre-DASH data, we sequenced the input of each of our RNA-
538 seq libraries before performing DASH on a MiSeq V2 Micro (Illumina). We tested DASHability on
539 a random subset of 200,000 paired-end reads chosen by seqtk (https://github.com/lh3/seqtk) from
540 each pre- and post-DASH library.
541
542 To map our RNA-seq data to *Bb*, we wanted to optimize for mapping reads that came from the
543 many paralogous gene families found across the plasmids of the genome. We used the
544 pseudoalignment tool Salmon v1.2.1 (Patro et al., 2017), which is used to accurately map reads
545 coming from different isoforms of the same gene, for this reason. While using Salmon to map to
546 CDS sequences may improve mapping to paralogous genes, it may also have a tradeoff of

547 reduced mapping of reads that fall on the ends of genes that reside in operons. Nevertheless, all
548 samples should be similarly affected, and any undercounting should not change differential
549 expression results. Reads were first trimmed of bases with quality scores less than 20 using Trim
550 Galore v0.6.5 (https://github.com/FelixKrueger/TrimGalore). We mapped our reads to *Bb* CDS
551 sequences as a reference transcriptome: NCBI Genbank GCA_000008685.2 ASM868v2 (with
552 plasmids lp5, cp9, and lp56 removed as they are not present in B31-S9) using Salmon with the
553 following parameters: --validateMappings --seqBias --gcBias. Before mapping, the transcriptome
554 was first indexed using the Salmon index command with the whole genome as decoys and the
555 parameter --keepDuplicates to keep all duplicate genes.
556
557 Read counts from Salmon were used as input into DESeq2 v1.24.0 (Love et al., 2014) for
558 differential expression analysis in R version 3.6.1. DESeq2 function PlotPCA() was used to create
559 a PCA plot from read counts after running the varianceStabilizingTransformation() function. For
560 differential expression analysis between days, a DESeq object was created from count data using
561 the DESeq() function. The lfcShrink() function with the apeglm method (Zhu et al., 2018) was
562 used to calculate fold changes between days. Code used for differential expression analysis is
563 available at https://github.com/annesapiro/Bb-tick-feeding.
564
565 **Gene classification**
566 To classify genes into functional groups, functional categories were sourced from Drecktrah et
567 al., 2015 where available. Other gene functions were sourced from Fraser et al., 1997. Genes
568 found within the co-transcribed "late" bacteriophage operon (Zhang and Marconi, 2005) were
569 considered "bacteriophage" even if their function is unknown. Outer surface lipoproteins were
570 those found in Dowdell et al., 2017 plus additional lipoproteins listed in Iyer et al., 2015 that were
571 found in Dowdell et al. 2017 categories SpII and SpI and evidence of outer surface localization.
572 Outer surface and periplasmic lipoproteins were classified as "cell envelope" in the absence of
573 other classifications. Gene family information from Casjens et al., 2000 was considered to aid in
574 classification.
575
576 **RT-qPCR measuring *Bb* enrichment**
577 To test the efficacy of our enrichment protocol, we used RT-qPCR to quantify *Bb flaB* and *I.*
578 *scapularis gapdh* transcript levels in enriched and depleted fractions. We synthesized cDNA from
579 8 µL of RNA extracted from *Bb* enrichment samples and their matched depleted samples from
580 feeding day 2, day 3, and day 4 using the qScript cDNA Synthesis Kit (Quantabio). cDNA was

581 diluted 2X before use in qPCR. To measure *flaB* copies, we created standards of known
582 concentration from purified PCR products. These standards were made from PCR with primers
583 with the following sequences: 5'-CACATATTCAGATGCAGACAGAGGTTCTA and 5'-
584 GAAGGTGCTGTAGCAGGTGCTGGCTGT. We ran a dilution series with ten-fold dilutions
585 between 10^6 copies and 10^1 copies of this PCR template alongside our enriched and depleted
586 samples. We performed qPCR using Taqman Universal PCR Master Mix (Applied Biosystems).
587 The primers used to amplify *flaB* were: 5'- TCTTTTCTCTGGTGAGGGAGCT and 5'-
588 TCCTTCCTGTTGAACACCCTCT (used at 900 nM) and the probe was /56-
589 FAM/AAACTGCTCAGGCTGCACCGGTTC/36-TAMSp (used at 250 nM). For tick *gapdh* RT-
590 qPCR, the cDNA samples were diluted an additional 2X. Standards of known concentration were
591 created using the qPCR primer sequences. Primer sequences were: 5'-
592 TTCATTGGAGACACCCACAG and 5'-CGTTGTCGTACCACGAGATAA (used at 900 nM). qPCR
593 was performed using PowerUp SYBR Green Master Mix (Applied Biosystems). For both *flaB* and
594 *gapdh*, the number of copies in each sample was calculated based on the standards of known
595 concentration. Three technical replicates were averaged from each of four biological replicates at
596 each time point tested. We totaled the number of copies in each matched enriched and depleted
597 fraction to calculate the fraction of *flaB* or *gapdh* that was found in either sample. All qPCR was
598 performed on the QuantStudio3 Real-Time PCR System (Applied Biosystems).
599
600 **Immunofluorescence microscopy**
601 To test whether the anti-*Bb* antibody recognized *Bb* inside of the tick, ticks at each day of feeding
602 were crushed in 50 µL of PBS. 10 µL of lysate was spotted onto slides and allowed to air dry
603 before slides were heated briefly three times over a flame. Heat fixed slides were then treated
604 with acetone for one hour. Slides were incubated with anti-*Bb* primary antibody (1:100 diluted in
605 PBS + 0.75% BSA) for 30 minutes at 37°C in a humid chamber. A control without primary antibody
606 was also used for each day. Slides were washed once in PBS for 15 minutes at room temperature,
607 then rinsed in distilled water and air dried. Anti-rabbit IgG Alexa 488 (Invitrogen) diluted 1:100 in
608 PBS + 0.75% BSA was added for 30 minutes at 37°C in a humid chamber. Slides were washed
609 in PBS for 15 minutes at room temperature three times, adding 1:100 Propidium Iodide
610 (Invitrogen) during the second wash. Slides were then rinsed with distilled water and air dried
611 before the addition of mounting media (Fluoromount-G, SouthernBiotech) and cover slips.
612 Fluorescence imaging was performed on a Nikon Ti2 inverted microscope for widefield
613 epifluorescence using a 100x/1.40 objective. Images were captured with NIS-Elements AR View

614 5.20 and then processed with ImageJ software (Schneider et al., 2012). No strong florescence
615 signal was observed on the control slides without primary antibody.
616
617 **Mass spectrometry of *Bb*-enriched samples**
618 To identify which tick proteins were found in samples after *Bb* enrichment across feeding, we fed
619 both uninfected and infected ticks on mice. We collected three replicates of uninfected ticks one
620 day after attachment (11 ticks per replicate), infected ticks one day after attachment (27 ticks per
621 replicate), uninfected ticks four days after attachment (8 ticks per replicate), and infected ticks
622 four days after attachment (16 ticks per replicate). Before anti-*Bb* enrichment, the uninfected tick
623 samples were mixed with *Bb* grown in culture that was washed with PBS (3 $x10^4$ *Bb* one day after
624 attachment and $3x10^6$ *Bb* four days after attachment) and mixed lysates were rotated at room
625 temperature for 30 minutes. Infected tick samples underwent the *Bb* enrichment process
626 immediately. The enrichment process followed the same protocol used for RNA-seq. Sample
627 volumes were increased to 1 mL as needed, and then 2 µL of anti-*Bb* antibody (Invitrogen: PA1-
628 73004; RRID: AB_1016668) was added, and samples were rotated at 4℃ for 30 minutes. 50 µL
629 of Dynabeads Protein G per sample were washed in PBS during this incubation and added to the
630 lysates, which were rotated at 4°C for 30 minutes. The beads were washed twice with 1 mL of
631 PBS, and then placed into 50 µL of lysis buffer (iST LYSE, PreOmics). Samples were boiled at
632 95°C for 5 minutes, and lysates were removed from beads and frozen for mass spectrometry
633 preparation.
634
635 For mass spectrometry, a nanoElute was attached in line to a timsTOF Pro equipped with a
636 CaptiveSpray Source (Bruker). Chromatography was conducted at 40°C through a 25 cm
637 reversed-phase C18 column (PepSep) at a constant flowrate of 0.5 µL min−1. Mobile phase A
638 was 98/2/0.1% water/MeCN/formic acid (v/v/v) and phase B was MeCN with 0.1% formic acid
639 (v/v). During a 108 min method, peptides were separated by a 3-step linear gradient (5% to 30%
640 B over 90 min, 30% to 35% B over 10 min, 35% to 95% B over 4 min) followed by a 4 min isocratic
641 flush at 95% for 4 min before washing and a return to low organic conditions. Experiments were
642 run as data-dependent acquisitions with ion mobility activated in PASEF mode. MS and MS/MS
643 spectra were collected with m/z 100 to 1700 and ions with z = +1 were excluded.
644
645 Raw data files were searched using PEAKS Online Xpro 1.6 (Bioinformatics Solutions Inc.). The
646 precursor mass error tolerance and fragment mass error tolerance were set to 20 ppm and 0.03
647 respectively. The trypsin digest mode was set to semi-specific and missed cleavages was set to

648 2. The *I. scapularis* reference proteome (Proteome ID UP000001555, taxon 6945) and *Bb*
649 reference proteome (Proteome ID UP000001807, strain ATCC 35210/B31) was downloaded from
650 Uniprot, totaling 21,774 entries. The *I. scapularis* proteome was the primary search reference and
651 the *Bb* was used as a secondary to identify any bacterial proteins present. Carbamidomethylation
652 was selected as a fixed modification. Oxidation (M) and Deamidation (NQ) was selected as a
653 variable modification. Experiments were performed in biological triplicate, with samples being a
654 single run on the instrument. Proteins present in a database search (−10 log(p-value) ≥ 20, 1%
655 peptide and protein FDR) were subjected to the following filtration process. We first filtered to
656 include proteins found in 2 out of 3 biological replicates, within each respective day (one or four
657 days after attachment). We calculated the mean area of proteins found in uninfected and infected
658 samples. Proteins with missing values (i.e. not identified in a sample) were set to 1. We calculated
659 the ratio of mean area for each protein as infected/uninfected, and enriched proteins were
660 identified by having a infected:uninfected ratio greater than 2 within their respective feeding day
661 (one or four days after attachment).
662
663 To classify the proteins we identified into functional groups, we used a PANTHER
664 Overrepresentation Test (released 07/12/2022) (Mi et al., 2019) with PANTHER version 17.0
665 (released 02/22/2022) (Thomas et al., 2022). We used all *Ixodes scapularis* genes in the database
666 as our reference list and analyzed the lists of proteins enriched on each day for their PANTHER
667 Protein Class. The test type used was Fisher's Exact, calculating a false discovery rate as the
668 correction.
669
670 Raw data files and searched datasets are available on the Mass Spectrometry Interactive Virtual
671 Environment (MassIVE), a full member of the Proteome Xchange consortium under the identifier:
672 MSV000090560.
673
674 **SUPPLEMENTAL TABLES**
675 **Table S1.** Overview of mapping statistics from 16 *Bb* sequencing samples.
676 **Table S2.** Differential expression analysis results between *in vitro* cultured *Bb* before and after
677 *Bb* enrichment.
678 **Table S3.** Transcriptome-wide differential expression analysis results from *Bb* across tick
679 feeding timepoints.
680 **Table S4.** Twofold differentially expressed *Bb* genes from across tick feeding timepoints.
681 **Table S5.** Transcripts per million (TPM) for all *Bb* genes across feeding timepoints.

682 **Table S6.** Mass spectrometry analysis for *Bb*-enriched samples.

683 **Table S7.** Annotation and GO term enrichment for tick proteins enriched on feeding day 1.

684 **Table S8.** Annotation and GO term enrichment for tick proteins enriched on feeding day 4.

685

686 **ACKNOWLEDGMENTS**

687 We are grateful to all members of the Chou lab for their feedback throughout the project and
688 specifically to Fauna Yarza and Patrick Rockefeller Grimes for assistance with tick feeding and
689 Ethel Enoex-Godonoo for administrative assistance. We thank Amy Lyden and Emily Crawford
690 for assistance with and reagents for DASH along with Olga Botvinnik and The Chan Zuckerberg
691 Biohub sequencing team for their input and sequencing assistance. We thank Patricia Rosa,
692 Jenny Wachter, Scott Samuels, and Meghan Lybecker for their feedback on the project. We also
693 thank William Hatleberg for assistance with figure schematics. This work was funded by: a Life
694 Sciences Research Foundation fellowship from the SVCF-Wave Fund to Anne Sapiro, a Beckman
695 Young Investigator award from the Arnold and Mabel Beckman Foundation to Balyn Zaro, grants
696 from CZ Biohub, the Pew Biomedical Research Foundation, and NIH funding 1R01AI132851 to
697 Seemay Chou, and NIH INBRE funding P20GM103474 to Patrick Secor and Margie Kinnersley.

698

699 **COMPETING INTERESTS**

700 Seemay Chou is president and CEO of Arcadia Biosciences.

701

702 **REFERENCES**

703 Barbour AG. 1988. Plasmid analysis of Borrelia burgdorferi, the Lyme disease agent. *J Clin*
704 *Microbiol* 26:475–478. doi:10.1128/jcm.26.3.475-478.1988

705 Barillas-Mury C, Ribeiro JMC, Valenzuela JG. 2022. Understanding pathogen survival and
706 transmission by arthropod vectors to prevent human disease. *Science* 377:eabc2757.
707 doi:10.1126/science.abc2757

708 Battisti JM, Bono JL, Rosa PA, Schrumpf ME, Schwan TG, Policastro PF. 2008. Outer Surface
709 Protein A Protects Lyme Disease Spirochetes from Acquired Host Immunity in the Tick
710 Vector. *Infect Immun* 76:5228–5237. doi:10.1128/iai.00410-08

711 Blevins JS, Hagman KE, Norgard MV. 2008. Assessment of decorin-binding protein A to the
712 infectivity of Borrelia burgdorferi in the murine models of needle and tick infection. *Bmc*
713 *Microbiol* 8:82. doi:10.1186/1471-2180-8-82

714 Caimano MJ, Dunham-Ems S, Allard AM, Cassera MB, Kenedy M, Radolf JD. 2015. Cyclic di-
715 GMP Modulates Gene Expression in Lyme Disease Spirochetes at the Tick-Mammal

716 Interface To Promote Spirochete Survival during the Blood Meal and Tick-to-Mammal
717 Transmission. *Infect Immun* 83:3043–3060. doi:10.1128/iai.00315-15

718 Caimano MJ, Groshong AM, Belperron A, Mao J, Hawley KL, Luthra A, Graham DE, Earnhart
719 CG, Marconi RT, Bockenstedt LK, Blevins JS, Radolf JD. 2019. The RpoS Gatekeeper in
720 Borrelia burgdorferi: An Invariant Regulatory Scheme That Promotes Spirochete Persistence
721 in Reservoir Hosts and Niche Diversity. *Front Microbiol* 10:1923.
722 doi:10.3389/fmicb.2019.01923

723 Caimano MJ, Iyer R, Eggers CH, Gonzalez C, Morton EA, Gilbert MA, Schwartz I, Radolf JD.
724 2007. Analysis of the RpoS regulon in Borrelia burgdorferi in response to mammalian host
725 signals provides insight into RpoS function during the enzootic cycle. *Mol Microbiol* 65:1193–
726 1217. doi:10.1111/j.1365-2958.2007.05860.x

727 Casjens S, Palmer N, Vugt RV, Huang WM, Stevenson B, Rosa P, Lathigra R, Sutton G,
728 Peterson J, Dodson RJ, Haft D, Hickey E, Gwinn M, White O, Fraser CM. 2000. A bacterial
729 genome in flux: the twelve linear and nine circular extrachromosomal DNAs in an infectious
730 isolate of the Lyme disease spirochete Borrelia burgdorferi. *Mol Microbiol* 35:490–516.
731 doi:10.1046/j.1365-2958.2000.01698.x

732 Casjens SR, Mongodin EF, Qiu W-G, Luft BJ, Schutzer SE, Gilcrease EB, Huang WM,
733 Vujadinovic M, Aron JK, Vargas LC, Freeman S, Radune D, Weidman JF, Dimitrov GI,
734 Khouri HM, Sosa JE, Halpin RA, Dunn JJ, Fraser CM. 2012. Genome Stability of Lyme
735 Disease Spirochetes: Comparative Genomics of Borrelia burgdorferi Plasmids. *Plos One*
736 7:e33280. doi:10.1371/journal.pone.0033280

737 Dowdell AS, Murphy MD, Azodi C, Swanson SK, Florens L, Chen S, Zückert WR. 2017.
738 Comprehensive Spatial Analysis of the Borrelia burgdorferi Lipoproteome Reveals a
739 Compartmentalization Bias toward the Bacterial Surface. *J Bacteriol* 199:e00658-16.
740 doi:10.1128/jb.00658-16

741 Drecktrah D, Lybecker M, Popitsch N, Rescheneder P, Hall LS, Samuels DS. 2015. The
742 Borrelia burgdorferi RelA/SpoT Homolog and Stringent Response Regulate Survival in the
743 Tick Vector and Global Gene Expression during Starvation. *Plos Pathog* 11:e1005160.
744 doi:10.1371/journal.ppat.1005160

745 Dunham-Ems SM, Caimano MJ, Pal U, Wolgemuth CW, Eggers CH, Balic A, Radolf JD. 2009.
746 Live imaging reveals a biphasic mode of dissemination of Borrelia burgdorferi within ticks. *J*
747 *Clin Invest* 119:3652–3665. doi:10.1172/jci39401

748 Dynerman D, Lyden A, Quan J, Caldera S, McGeever A, Dimitrov B, King R, Cirolia G, Tan M,
749 Sit R, Berge M van den, Kerstjens HAM, Faiz A, Christenson S, Langelier C, DeRisi J,
750 Crawford E. 2020. Designing and implementing programmable depletion in sequencing
751 libraries with DASHit. *Biorxiv* 2020.01.12.891176. doi:10.1101/2020.01.12.891176

752 Edgar R, Domrachev M, Lash AE. 2002. Gene Expression Omnibus: NCBI gene expression
753 and hybridization array data repository. *Nucleic Acids Res* 30:207–210.
754 doi:10.1093/nar/30.1.207

755 Eggers CH, Samuels DS. 1999. Molecular evidence for a new bacteriophage of Borrelia
756 burgdorferi. *J Bacteriol* 181:7308–13.

757 Fraser CM, Casjens S, Huang WM, Sutton GG, Clayton R, Lathigra R, White O, Ketchum KA,
758 Dodson R, Hickey EK, Gwinn M, Dougherty B, Tomb J-F, Fleischmann RD, Richardson D,
759 Peterson J, Kerlavage AR, Quackenbush J, Salzberg S, Hanson M, Vugt R van, Palmer N,
760 Adams MD, Gocayne J, Weidman J, Utterback T, Watthey L, McDonald L, Artiach P,
761 Bowman C, Garland S, Fujii C, Cotton MD, Horst K, Roberts K, Hatch B, Smith HO, Venter
762 JC. 1997. Genomic sequence of a Lyme disease spirochaete, Borrelia burgdorferi. *Nature*
763 390:580–586. doi:10.1038/37551

764 Gilmore RD, Howison RR, Dietrich G, Patton TG, Clifton DR, Carroll JA. 2010. The bba64 gene
765 of Borrelia burgdorferi, the Lyme disease agent, is critical for mammalian infection via tick
766 bite transmission. *P Natl Acad Sci Usa* 107:7515–20. doi:10.1073/pnas.1000268107

767 Gilmore RD, Mbow ML, Stevenson B. 2001. Analysis of Borrelia burgdorferi gene expression
768 during life cycle phases of the tick vector Ixodes scapularis. *Microbes Infect* 3:799–808.
769 doi:10.1016/s1286-4579(01)01435-6

770 Gu W, Crawford ED, O'Donovan BD, Wilson MR, Chow ED, Retallack H, DeRisi JL. 2016.
771 Depletion of Abundant Sequences by Hybridization (DASH): using Cas9 to remove
772 unwanted high-abundance species in sequencing libraries and molecular counting
773 applications. *Genome Biol* 17:41. doi:10.1186/s13059-016-0904-5

774 Haas BJ, Chin M, Nusbaum C, Birren BW, Livny J. 2012. How deep is deep enough for RNA-
775 Seq profiling of bacterial transcriptomes? *Bmc Genomics* 13:734. doi:10.1186/1471-2164-13-
776 734

777 He M, Ouyang Z, Troxell B, Xu H, Moh A, Piesman J, Norgard MV, Gomelsky M, Yang XF.
778 2011. Cyclic di-GMP is Essential for the Survival of the Lyme Disease Spirochete in Ticks.
779 *Plos Pathog* 7:e1002133. doi:10.1371/journal.ppat.1002133

780 Hübner A, Yang X, Nolen DM, Popova TG, Cabello FC, Norgard MV. 2001. Expression of
781 Borrelia burgdorferi OspC and DbpA is controlled by a RpoN–RpoS regulatory pathway. *Proc*
782 *National Acad Sci* 98:12724–12729. doi:10.1073/pnas.231442498

783 Iyer R, Caimano MJ, Luthra A, Axline D, Corona A, Iacobas DA, Radolf JD, Schwartz I. 2015.
784 Stage-specific global alterations in the transcriptomes of Lyme disease spirochetes during
785 tick feeding and following mammalian host adaptation. *Mol Microbiol* 95:509–538.
786 doi:10.1111/mmi.12882

787 Kasumba IN, Bestor A, Tilly K, Rosa PA. 2016. Virulence of the Lyme disease spirochete before
788 and after the tick bloodmeal: a quantitative assessment. *Parasite Vector* 9:129.
789 doi:10.1186/s13071-016-1380-1

790 Kenedy MR, Lenhart TR, Akins DR. 2012. The role of Borrelia burgdorferi outer surface
791 proteins. *Fems Immunol Medical Microbiol* 66:1–19. doi:10.1111/j.1574-695x.2012.00980.x

792 Kovacs-Simon A, Titball RW, Michell SL. 2010. Lipoproteins of Bacterial Pathogens. *Infect*
793 *Immun* 79:548–561. doi:10.1128/iai.00682-10

794 Kurokawa C, Lynn GE, Pedra JHF, Pal U, Narasimhan S, Fikrig E. 2020. Interactions between
795 Borrelia burgdorferi and ticks. *Nat Rev Microbiol* 1–14. doi:10.1038/s41579-020-0400-5

796 Love MI, Huber W, Anders S. 2014. Moderated estimation of fold change and dispersion for
797 RNA-seq data with DESeq2. *Genome Biol* 15:550. doi:10.1186/s13059-014-0550-8

798 Lyden A, Crawford E, Quan J, Caldera S, Dynerman D. 2019a. DASH Protocol v4.
799 doi:10.17504/protocols.io.6rjhd4n

800 Lyden A, Crawford E, Quan J, Caldera S, Pesce-Ares L. 2019b. In Vitro Transcription for
801 dgRNA v2. doi:10.17504/protocols.io.3bpgimn

802 Manning JE, Cantaert T. 2019. Time to Micromanage the Pathogen-Host-Vector Interface:
803 Considerations for Vaccine Development. *Nato Adv Sci Inst Se* 7:10.
804 doi:10.3390/vaccines7010010

805 Mi H, Muruganujan A, Huang X, Ebert D, Mills C, Guo X, Thomas PD. 2019. Protocol Update for
806 large-scale genome and gene function analysis with the PANTHER classification system
807 (v.14.0). *Nat Protoc* 14:703–721. doi:10.1038/s41596-019-0128-8

808 Ohnishi J, Piesman J, Silva AM de. 2001. Antigenic and genetic heterogeneity of Borrelia
809 burgdorferi populations transmitted by ticks. *Proceedings of the National Academy of*
810 *Sciences* 98:670–5. doi:10.1073/pnas.98.2.670

811 Ojaimi C, Mulay V, Liveris D, Iyer R, Schwartz I. 2005. Comparative Transcriptional Profiling of
812 Borrelia burgdorferi Clinical Isolates Differing in Capacities for Hematogenous Dissemination.
813 *Infect Immun* 73:6791–6802. doi:10.1128/iai.73.10.6791-6802.2005

814 Pal U, Kitsou C, Drecktrah D, Yaş OB, Fikrig E. 2022. Interactions Between Ticks and Lyme
815 Disease Spirochetes. *Curr Issues Mol Biol* 42:113–144. doi:10.21775/cimb.042.113

816 Pal U, Li X, Wang T, Montgomery RR, Ramamoorthi N, deSilva AM, Bao F, Yang X, Pypaert M,
817 Pradhan D, Kantor FS, Telford S, Anderson JF, Fikrig E. 2004. TROSPA, an Ixodes
818 scapularis Receptor for Borrelia burgdorferi. *Cell* 119:457–468.
819 doi:10.1016/j.cell.2004.10.027

820 Patro R, Duggal G, Love MI, Irizarry RA, Kingsford C. 2017. Salmon provides fast and bias-
821 aware quantification of transcript expression. *Nat Methods* 14:417 419.
822 doi:10.1038/nmeth.4197

823 Patton TG, Brandt KS, Nolder C, Clifton DR, Carroll JA, Gilmore RD. 2013. Borrelia burgdorferi
824 bba66 Gene Inactivation Results in Attenuated Mouse Infection by Tick Transmission. *Infect*
825 *Immun* 81:2488–2498. doi:10.1128/iai.00140-13

826 Phelan JP, Kern A, Ramsey ME, Lundt ME, Sharma B, Lin T, Gao L, Norris SJ, Hyde JA, Skare
827 JT, Hu LT. 2019. Genome-wide screen identifies novel genes required for Borrelia
828 burgdorferi survival in its Ixodes tick vector. *Plos Pathog* 15:e1007644.
829 doi:10.1371/journal.ppat.1007644

830 Radolf JD, Caimano MJ, Stevenson B, Hu LT. 2012. Of ticks, mice and men: understanding the
831 dual-host lifestyle of Lyme disease spirochaetes. *Nat Rev Microbiol* 10:87 99.
832 doi:10.1038/nrmicro2714

833 Rego ROM, Bestor A, Rosa PA. 2011. Defining the Plasmid-Borne Restriction-Modification
834 Systems of the Lyme Disease Spirochete Borrelia burgdorferi. *J Bacteriol* 193:1161–1171.
835 doi:10.1128/jb.01176-10

836 Rego ROM, Bestor A, Štefka J, Rosa PA. 2014. Population Bottlenecks during the Infectious
837 Cycle of the Lyme Disease Spirochete Borrelia burgdorferi. *Plos One* 9:e101009.
838 doi:10.1371/journal.pone.0101009

839 Revel AT, Talaat AM, Norgard MV. 2002. DNA microarray analysis of differential gene
840 expression in Borrelia burgdorferi, the Lyme disease spirochete. *Proc National Acad Sci*
841 99:1562–1567. doi:10.1073/pnas.032667699

842 Ring K, Couper LI, Sapiro AL, Yarza F, Yang XF, Clay K, Mateusiak C, Chou S, Swei A. 2022.
843 Host blood meal identity modifies vector gene expression and competency. *Mol Ecol*
844 31:2698–2711. doi:10.1111/mec.16413

845 Rosenberg R, Lindsey NP, Fischer M, Gregory CJ, Hinckley AF, Mead PS, Paz-Bailey G,
846 Waterman SH, Drexler NA, Kersh GJ, Hooks H, Partridge SK, Visser SN, Beard CB,
847 Petersen LR. 2018. Vital Signs: Trends in Reported Vectorborne Disease Cases — United
848 States and Territories, 2004–2016. *Morbidity Mortal Wkly Rep* 67:496–501.
849 doi:10.15585/mmwr.mm6717e1

850 Samuels DS, Lybecker MC, Yang XF, Ouyang Z, Bourret TJ, Boyle WK, Stevenson B,
851 Drecktrah D, Caimano MJ. 2021. Gene Regulation and Transcriptomics. *Curr Issues Mol Biol*
852 42:223–266. doi:10.21775/cimb.042.223

853 Schneider CA, Rasband WS, Eliceiri KW. 2012. NIH Image to ImageJ: 25 years of image
854 analysis. *Nat Methods* 9:671–675. doi:10.1038/nmeth.2089

855 Schwartz I, Margos G, Casjens SR, Qiu W-G, Eggers CH. 2021. Multipartite Genome of Lyme
856 Disease Borrelia : Structure, Variation and Prophages. *Curr Issues Mol Biol* 42:409–454.
857 doi:10.21775/cimb.042.409

858 Shaw WR, Catteruccia F. 2018. Vector biology meets disease control: using basic research to
859 fight vector-borne diseases. *Nat Microbiol* 4:20–34. doi:10.1038/s41564-018-0214-7

860 Spielman A, Ribeiro JMC, Mather TN, Piesman J. 1987. Dissemination and Salivary Delivery of
861 Lyme Disease Spirochetes in Vector Ticks (Acari: Ixodidae). *J Med Entomol* 24:201–205.
862 doi:10.1093/jmedent/24.2.201

863 Steere AC, Sikand VK, Meurice F, Parenti DL, Fikrig E, Schoen RT, Nowakowski J, Schmid CH,
864 Laukamp S, Buscarino C, Krause DS. 1998. Vaccination against Lyme Disease with
865 Recombinant Borrelia burgdorferi Outer-Surface Lipoprotein A with Adjuvant. *New Engl J*
866 *Medicine* 339:209–215. doi:10.1056/nejm199807233390401

867 Steere AC, Strle F, Wormser GP, Hu LT, Branda JA, Hovius JWR, Li X, Mead PS. 2016. Lyme
868 borreliosis. *Nat Rev Dis Primers* 2:nrdp201690. doi:10.1038/nrdp.2016.90

869 Stevenson B, Zückert WR, Akins DR. 2000. Repetition, conservation, and variation: the multiple
870 cp32 plasmids of Borrelia species. *J Mol Microb Biotech* 2:411–22.

871 Thomas PD, Ebert D, Muruganujan A, Mushayahama T, Albou L, Mi H. 2022. PANTHER:
872 Making genome-scale phylogenetics accessible to all. *Protein Sci* 31:8–22.
873 doi:10.1002/pro.4218

874 Tilly K, Rosa PA, Stewart PE. 2008. Biology of Infection with Borrelia burgdorferi. *Infect Dis Clin*
875 *N Am* 22:217 234. doi:10.1016/j.idc.2007.12.013

876 Tokarz R, Anderton JM, Katona LI, Benach JL. 2004. Combined Effects of Blood and
877 Temperature Shift on Borrelia burgdorferi Gene Expression as Determined by Whole
878 Genome DNA Array. *Infect Immun* 72:5419–5432. doi:10.1128/iai.72.9.5419-5432.2004

879 Zhang H, Marconi RT. 2005. Demonstration of Cotranscription and 1-Methyl-3-Nitroso-
880 Nitroguanidine Induction of a 30-Gene Operon of Borrelia burgdorferi: Evidence that the 32-
881 Kilobase Circular Plasmids Are Prophages. *J Bacteriol* 187:7985–7995.
882 doi:10.1128/jb.187.23.7985-7995.2005

883 Zhang L, Zhang Y, Adusumilli S, Liu L, Narasimhan S, Dai J, Zhao YO, Fikrig E. 2011.
884 Molecular Interactions that Enable Movement of the Lyme Disease Agent from the Tick Gut
885 into the Hemolymph. *Plos Pathog* 7:e1002079. doi:10.1371/journal.ppat.1002079

886 Zhu A, Ibrahim JG, Love MI. 2018. Heavy-tailed prior distributions for sequence count data:
887 removing the noise and preserving large differences. *Bioinformatics* 35:2084–2092.
888 doi:10.1093/bioinformatics/bty895

889